Available online at www.sciencedirect.com
ScienceDirect
Journal of Power Sources 164 (2007) 24–32
JOURNAL OF POWER SOURCES
www.elsevier.com/locate/jpowsour

Sintering behavior of porous α-lithium aluminate matrices in molten carbonate fuel cells at high temperature

Li Zhou [a,b,*], Huaxin Lin [a], Baolian Yi [a]

[a] *Laboratory of Fuel Cells, Dalian Institute of Chemical Physics, Chinese Academy of Sciences, Dalian 116023, China*
[b] *Graduate School of the Chinese Academy of Sciences, Beijing 100039, China*

Received 26 August 2006; received in revised form 8 October 2006; accepted 9 October 2006
Available online 27 November 2006

Abstract

By conducting experiments under pressures on the matrix of a single molten carbonate fuel cell (MCFC), as well as by performing comparative sintering experiments with and without the molten carbonate, changes in the maximum pore diameter, pore-size distribution, crystalline phase, Brunauer–Emmett–Teller (BET) surface area and surface configuration were measured. The parameters of the effectiveness of the gas barrier ($\Delta P \geq 0.1$ MPa) and the porosity ($40\% \leq \delta \leq 70\%$) were taken as lifetime criteria for the matrix. By using regression equations based on the experimental results, the matrix was estimated by two aspects: maximum pore diameter and porosity for commercial requirements. Meanwhile, changes in the maximum pore diameter, pore-size distribution and porosity for estimating the sintering behavior were presented and explained theoretically. Rearrangements, slips and dissolutions of the α-lithium aluminate (α-$LiAlO_2$) particles were observed in the matrices, which promote the alteration of the pore diameter and porosity during the sintering processes.

Keywords: Porous ceramic; Sintering behavior; Lifetime criterion; α-Lithium aluminate (α-$LiAlO_2$) matrix; Pore structure

1. Introduction

There are several advantages of molten carbonate fuel cells (MCFCs) due to their high operating temperature (650 °C), which include high efficiency and a cogeneration capability [1], when compared to low-temperature fuel cells. MW class MCFC power systems are promising for use as major electric power plants in the future [2,3]. For the commercialization of a MCFC, however, some technical problems have to be solved in order to improve the performance of the MCFC system. For example, the gas pressure difference between the anode and the cathode may damage the cell due to gas crossover through the matrix [4]. In general, gas crossover is caused by two reasons: (1) changes in the characteristics of the matrix, including the pore diameter and the porosity; (2) depleting of the electrolyte due to volatilization and corrosion in the cell. Accordingly, the inert and porous lithium aluminate ($LiAlO_2$) ceramic matrix of a MCFC should have a high capability to retain the molten electrolyte and prevent gas crossover and have a good pore stability.

Some researchers have studied the growth and phase transformation of $LiAlO_2$ particles in molten carbonate [5–12], but few have dealt with the matrix of the MCFC, especially the pore structure of the matrix. Tomimatsu et al. [5] found that α-$LiAlO_2$ particles did not grow much at high temperature in the electrolyte for over 7550 h. The sintering behavior of the α-$LiAlO_2$ particles is different from that of γ-$LiAlO_2$ particles in the matrix, but little information has been reported. Hatoh et al. [6] have studied the behavior of the γ-$LiAlO_2$ matrix sintered under MCFC conditions and found that the size of the γ-$LiAlO_2$ particles remained stable at lower temperatures in molten carbonate with high Li/K ratios, and under high CO_2 partial pressure. Sotouchi et al. [11] studied the growth mechanism of $LiAlO_2$ particles sintered in molten carbonate and gave some explanations for the size of $LiAlO_2$ particles being kept constant. Takizawa and Hagiwara [12] have further investigated the effect of certain factors on the difference in the changes of particle size and phase transformation between the α-$LiAlO_2$ and γ-$LiAlO_2$. Veringa [7] put forward a theoretical model to simulate the instability and rearrangement of solid particles sintered at higher temperature,

* Corresponding author at: Laboratory of Fuel Cells, Dalian Institute of Chemical Physics, Chinese Academy of Sciences, Dalian 116023, China. Tel.: +86 411 84379103; fax: +86 411 84684839.
E-mail address: zhouli@dicp.cn (L. Zhou).

0378-7753/$ – see front matter © 2006 Published by Elsevier B.V.
doi:10.1016/j.jpowsour.2006.10.043

but he did not provide more experimental results to confirm his theoretical views.

In this work, the sintering behavior of the pore structure of porous ceramic matrices has been investigated in two aspects: the pore diameter and the porosity. The maximum pore diameter, the pore-size distribution and the porosity have been found to change with the sintering time. We have proposed the rearrangement and slip of α-$LiAlO_2$ particles, to explain the experimental phenomena.

2. Experimental

2.1. Preparation of α-$LiAlO_2$ powder and matrices

Coarse α-$LiAlO_2$ powder was prepared by the reaction of Li_2CO_3 (A.P., Xinhua Chemical Reagent Factory, Beijing, China) with α-Al_2O_3 (A.P., Chengdu Chemical Reagent Factory, China) at 700 °C. Before the reaction, Li_2CO_3 and α-Al_2O_3 were mixed sufficiently by ball-mill treatment. Fine α-$LiAlO_2$ powder was prepared by "chloride" synthesis method [13]. The mean particle sizes of the coarse and fine α-$LiAlO_2$ powders were 2.89 and 0.32 μm, respectively. The α-$LiAlO_2$ powder in a ratio of coarse powder to fine powder was mixed with the polyvinyl butyral (PVB) binder and other organic additives, such as a solvent, plasticizer, dispersant and an anti-bubbling agent. The mixture was ball-milled into a paste for 100–120 h. Then the matrices were prepared by tape casting using a doctor-blade [14]. Finally they were dried and thermally pressed into cell matrices.

2.2. Measurements of the maximum pore diameter in porous ceramic matrices

Measurements were conducted in situ in a single cell of MCFC. A sintered porous Ni–Cr plate and a Ni plate were used as the anode and cathode, respectively, and the eutectic melt ($0.62Li_2CO_3 + 0.38K_2CO_3$) was used as the electrolyte. An α-$LiAlO_2$ matrix sandwiched between the anode and cathode was assembled into a single MCFC cell. The areas of the anode, cathode and the matrix were 28, 28 and 50 cm^2, respectively. Their thicknesses were 0.40, 0.40 and 0.89 mm, and porosities were 60–63, 60–63 and 55–56%, respectively. The mean pore diameters in the cathode (which was oxidized in situ into NiO), the anode and the matrix were 18–26, 18–25 and 0.36 μm, respectively.

The cell was heated slowly and at the same time oxygen gas was introduced into the cathode and the anode chamber. In this way organic additives volatilized and PVB was burnt out from the matrix in an oxygen atmosphere [14]. After the burning out of the organic compounds in the matrix, it turned into a porous ceramic plate. When the temperature was about 500 °C, the electrolyte pre-stored in the cathode chamber began to melt gradually and impregnated the porous ceramic matrix by capillary action. After the matrix was fully impregnated with the electrolyte, it became a sealed and ionic conductor layer. Then the porous ceramic matrix was the support frame and the molten carbonate anion (CO_3^{2-}) was the charge carrier.

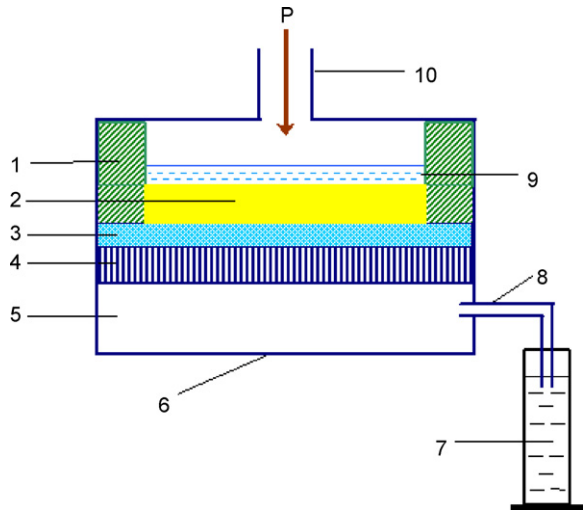

Fig. 1. Measurement of maximum pore diameter in matrix by the pool at room temperature. (1) Rubber; (2) the matrix; (3) porous sintered Ni plate; (4) porous support plate; (5) cavity; (6) pool body; (7) water; (8) capillary; (9) absolute alcohol; (10) inlet tube.

N_2 was employed as the measuring gas which passed through the cathode and anode chamber at 650 °C. Initially the flow was zero at the anode inlet. Then the N_2 pressure in the cathode chamber was elevated, and the flow was checked at the anode exit by a bubbler. Once N_2 crossover was found to occur, the minimum pressure difference ΔP between the cathode and anode chamber was measured easily. The maximum pore diameter in the matrix was calculated from the measured ΔP by the Yong–Laplace equation [15]. The measurement medium was the electrolyte ($0.62Li_2CO_3 + 0.38K_2CO_3$), its surface tension coefficient, σ, was 0.198 N m^{-1} at 650 °C [16].

The measurement was also conducted at room temperature, as shown in Fig. 1. The matrix was heated slowly in air out-of-cell, so that the organic additives volatilized and the PVB burnt out from the matrix. After the burning out of the organic compounds, the matrix became a porous ceramic plate, which was then assembled into the pool. The measuring and calculating method were the same as presented above, except that alcohol was used as the measuring medium instead of the ($0.62Li_2CO_3 + 0.38K_2CO_3$) electrolyte, and its surface tension coefficient, σ, was 0.02239 N m^{-1} at room temperature [16].

2.3. Physicochemical characterization of the porous ceramic matrices

After the burn-out of the organic compounds, the porous ceramic matrices were used for measurement. Some matrices were fully impregnated with the molten carbonate electrolyte and sintered in α-Al_2O_3 crucibles, while others were sintered in the same manner, but without impregnating the electrolyte. All matrices were sintered under an ambient pressure of N_2 at 650 °C.

Since the matrices could not be separated from the frozen carbonate salts after sintering in the molten carbonate, pore-size distributions and porosity of the matrices could not be measured

directly. They were first washed with a mixture of acetic acid and acetic anhydride (1:1, mole ratio) and then washed with ethanol. After drying, the pore frames of the matrices were collapsed, and α-$LiAlO_2$ powder was obtained. Consequently, only Brunauer–Emmett–Teller (BET) surface areas could be measured for the matrices sintered in the electrolyte.

The crystalline phases of α-$LiAlO_2$ particles were characterized by X-ray diffraction (XRD) (DMX-RBX-diffraction instrument, Japan). The BET surface areas were measured by a physical absorption apparatus (Quanten Chrome, Autosorb-1, USA). The surface morphologies of the matrices were observed by scanning electron microscopy (SEM) (JEM-1200EX type, Japan). The porosities of the matrices sintered without impregnating the electrolyte were measured by Hg intrusion apparatus (Carlo Erba Strumen-tazione Microstructure Lab 2000 type, Italy).

3. Results and discussion

3.1. Crystalline phase and surface morphology of the matrices

The results of XRD analysis of several samples are shown in Fig. 2. It was demonstrated that the crystalline phase of α-$LiAlO_2$ remained unchanged during the washing of the sample with the mixture of acetic acid and acetic anhydride. It also can be seen that the phase of α-$LiAlO_2$ remained unchanged during the sintering process, no matter how it was sintered with or without molten carbonate electrolyte. The crystalline phase of all the samples measured were α-phase $LiAlO_2$, and no phase transformation was observed.

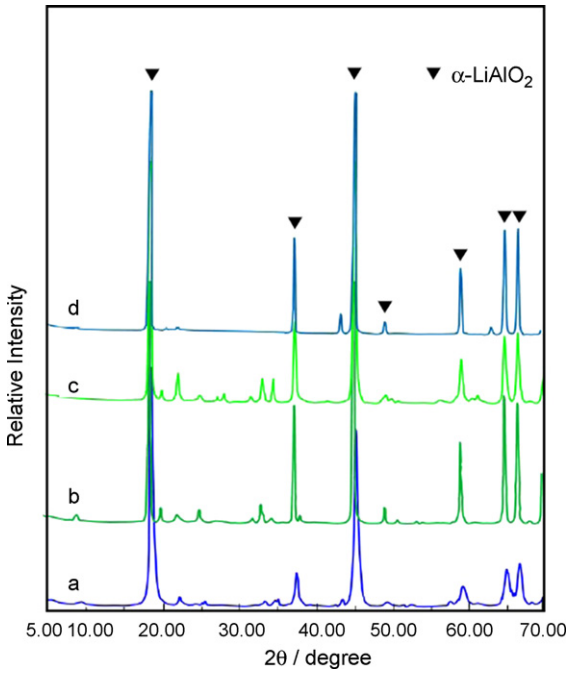

Fig. 2. XRD patterns. (a) Sintered for 1 h; (b) sintered for 1 h and after treating with organic solvent; (c) sintered for 4500 h without impregnating the electrolyte; (d) sintered for 4000 h in electrolyte.

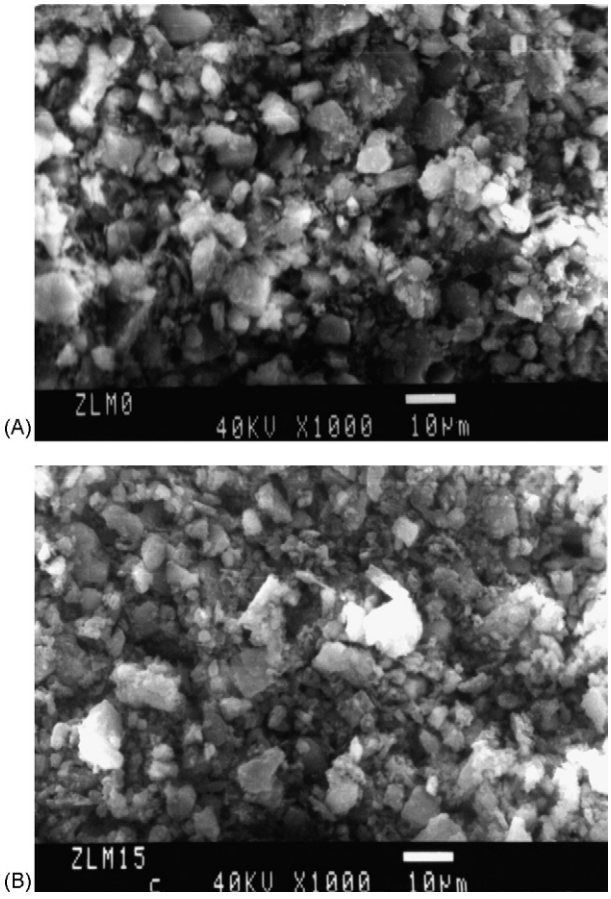

Fig. 3. The SEM micrographs on the surface of the matrix sintered without impregnating the electrolyte under the ambient pressure of N_2. (A) Sintered for 1 h; (B) sintered for 4500 h.

Fig. 3 shows SEM photographs of the surfaces of the matrices sintered for 1 and 4500 h without impregnating with electrolyte under an ambient pressure of N_2. It is obvious that there was almost no morphological change of the surface of the matrix after being sintered for 4500 h, and the particle size remained at the same level for the matrices sintered from 1 to 4500 h. However, this is not an essential requirement for molten carbonate fuel cells, and it does not imply that the pore structure in the matrices does not change.

3.2. Maximum pore diameter in the porous ceramic matrices of a cell

In practical operations, the permissible maximum pressure difference between the anode and cathode chambers should be less than 0.1 MPa, which depends on the maximum pore diameter of the matrix, since gas crossover will first occur through the maximum pores. According to the Yong–Laplace equation [15],

$$\Delta P = \frac{2\sigma \cos\theta}{\gamma} \quad (1)$$

where σ is the surface tension coefficient of the electrolyte, θ the contact angle between the electrolyte and the α-$LiAlO_2$ matrix, γ

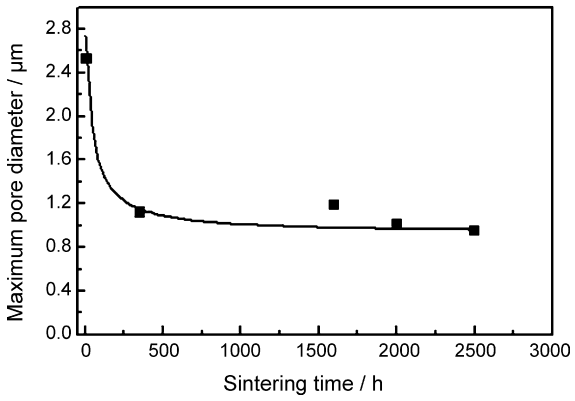

Fig. 4. Alteration of maximum pore diameter in matrix with sintering time. Solid line (—), the line according to the regression Eq. (2). Solid symbols (■), the measured data in the experiments.

the maximum pore radius in the matrix and ΔP is the N_2 pressure penetrating the maximum pore in the matrix impregnated with electrolyte at 650 °C.

The maximum pore diameter in the matrix can be calculated from the measured ΔP. If the safety limit of the gas pressure difference is 0.1 MPa, the maximum pore diameter is calculated to be 7.92 μm according to Eq. (1). Hence, the maximum pore diameter in the matrix should be less than 7.92 μm. Thus, the maximum pore diameter of 7.92 μm can be used as a lifetime criterion of the matrix. If the maximum pore diameter is larger than 7.92 μm, the cell will be damaged.

The alteration of the maximum pore diameter in the matrices with sintering time in the cell is shown in Fig. 4. At the beginning of the sintering process for the matrix, the maximum pore diameter in the matrix was 2.69 μm, which was the largest of measured. It altered with sintering time and then became smaller, ~1.0 μm.

The regression equations derived from the experimental results is as follows,

$$D_m = \frac{2.75258 + 0.01929t}{1 + 0.02072t} \quad (2)$$

where D_m is the maximum pore diameter in the matrix (μm) and t is the sintering time (h).

By Eq. (2), the maximum pore diameter in the matrix can be calculated against sintering time, as shown in Table 1 and Fig. 4. The calculated maximum pore diameter decreased gradually with sintering time, but it was still much less than 7.92 μm.

3.3. Porosities in the porous ceramic matrices

In order to meet the requirement of good conductivity of the molten carbonate electrolyte in the matrix, the porosity of the matrix should be in a suitable range. According to Meredith–Tobias equation [17],

$$\rho = \rho_0 \delta^{-2} \quad (3)$$

where ρ is the specific resistance of the matrix, ρ_0 the specific resistance of the electrolyte ($0.62Li_2CO_3 + 0.38K_2CO_3$) at 650 °C, which was 0.5767 Ω cm and δ is the matrix porosity.

A relationship between the resistance across the matrix and the matrix porosity can be established. The matrix porosity should be located within a suitable range of $40\% \leq \delta \leq 70\%$ [17], which can be used as a lifetime criterion of the matrix porosity. If the matrix porosity δ is lower than 40%, ohmic drop (IR) across the matrix will be higher, thus the cell performance will decay sharply. If the matrix porosity δ is higher than 70%, the storage capacity of the electrolyte impregnated into the matrix will be increased. However, if the matrix porosity δ is higher than 70%, the amount of the organic compounds in the matrix will have to be increased in the preparation process of the matrix, and they will tend to agglomerate, then the maximum pore diameter will be larger than 7.92 μm after sintering of the matrix. If the matrix porosity δ is approaching 70% during the sintering process of the matrix or during the operation of the MCFC, defects and larger pores will be created by rearrangements and slips of the particles in the matrix. Since the pore size in the matrix is less than that in the electrodes, when the matrix porosity δ is increased to above 70%, the electrolyte will be redistributed to satisfy the capillary force equilibrium among the cell components, and some electrolyte in the electrodes will move into the matrix by capillary force. Thus, the triple phase boundaries (TPB) in the electrode will be changed, and even the cell performance will be diminished [1,16–18]. Higher porosity (70%) will cause problems, and diminish the cell performance.

The relationship between the porosity of a matrix sintered without impregnating with the electrolyte and the sintering time is illustrated in Fig. 5. The regression equations can be derived from their porosities, which are shown as follows,

$$\delta_W = 55.332 + 1.876 \times 10^{-4} t \quad (4)$$

where δ_W is the porosity in the matrix sintered without impregnating with the electrolyte (%) and t is the sintering time (h).

As shown in Fig. 5, the porosities of the matrices sintered without impregnating with the electrolyte increased gradually with the sintering time from 1 to 4500 h. The porosities of the matrices sintered for a longer time can be estimated by Eq. (4), and the results are listed in Table 2.

The BET surface areas, the porosities and the pore-size distribution were measured for the matrices sintered without impregnating with the electrolyte. But only the BET surface areas were measured for the matrices sintered in the electrolyte, and the

Table 1
The results of measurement and calculation of maximum pore diameter in the matrix with sintering time

Sintering time (h)	1	500	1000	10000	20000	30000	40000
D_m (μm)	2.69	1.09	1.01	0.94	0.94	0.93	0.93

D_m, the maximum pore diameter in the matrix.

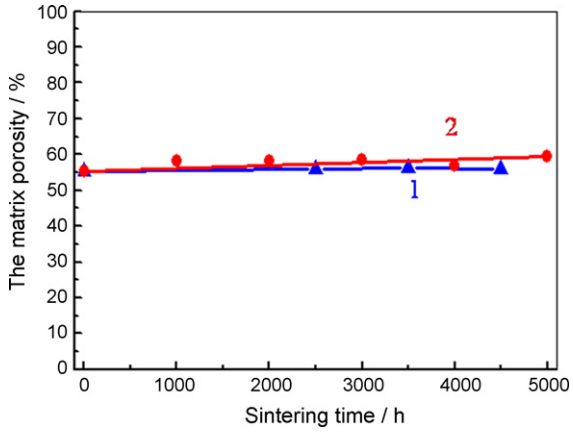

Fig. 5. Alteration of matrix porosity with sintering time. Solid symbols (▲) and line (1), the porosity of matrix sintered without impregnating the electrolyte; solid symbols (●) and line (2), the porosity of matrix sintered in the electrolyte.

porosities could not be directly measured. So, it is necessary to obtain a relationship between the BET surface area and the porosity of the matrix sintered in the electrolyte, and then we can deduce the relationship between the porosity and the sintering time.

Considering the shape and the size distributions of the particles and the types of particle packing in the matrices of the MCFC, Kinoshita and Kucera [19] have assumed that the pore shape in the matrix was cylindrical, and he deduced the equation (i.e. "Eq. (17)" in ref. [19]) to present the relationship between the BET surface area and the porosity of the matrix sintered in the electrolyte as follows,

$$r_p = \frac{2\delta}{d_p S(1-\delta)} \tag{5}$$

where r_p is the pore radius in the α-$LiAlO_2$ matrix, δ the porosity in the α-$LiAlO_2$ matrix, d_p the density of the α-$LiAlO_2$ particle and S is the surface area of the α-$LiAlO_2$ particle.

Here, if the density of the particles is assumed to be constant in Eq. (5) during the measuring and calculating of the porosity, then the porosity of the matrix will be corresponding to the BET surface area of particles of the same sample at the same sintering time. The relationship is simply expressed as follows,

$$\frac{1}{\delta} - \frac{k}{S} = 1 \tag{6}$$

where k is a function of the sintering time and equals $2/(r_p \times d_p)$ at a sintering time.

So the relationship between the BET surface area and the porosity should be established by the measured results of the samples sintered without impregnating with the electrolyte according to Eq. (6).

The porosities of the matrices sintered in the electrolyte can be obtained by using their measured BET surface areas from the above-mentioned relationship. The relationship between the porosity of the matrix sintered in electrolyte and the sintering time can be deduced according to Eq. (6), which is also shown in Fig. 5. The regression equations can be derived from their porosity as follows,

$$\delta_E = 56.042 + 2.666 \times 10^{-4} t \tag{7}$$

where δ_E is the porosity in the matrix sintered in the electrolyte (%) and t is the sintering time (h).

As shown in Fig. 5, the porosities of the matrices sintered in the electrolyte increases with the sintering time from 1 to 5000 h, but it is lightly higher than those in the matrix sintered without impregnating with the electrolyte. The porosities of the matrices sintered for a longer time can be estimated by "Eq. (7)", as listed in Table 2. They both can be lower than 70%, the upper-limit of the lifetime criterion of the matrix porosity.

The matrix with good stability should match the two criteria of the maximum pore diameter and porosity at the same time; otherwise the lifetime of the matrix would be reduced. The lifetime of the α-$LiAlO_2$ ceramic matrix can be estimated with the two criteria based on the experimental results and the regression equations.

3.4. Rearrangement of the α-$LiAlO_2$ particles through slips in the matrices

3.4.1. Rearrangements through slips

The maximum pore diameter in the matrix can be measured as shown in Fig. 1. From the Young–Laplace equation, the measured results could be obtained and are listed in Table 3. The results measured in situ with a single cell of MCFC are demonstrated in Fig. 4. By comparing the measured results in Table 3 and Fig. 4, it can be found that the measured maximum pore diameter changed in the initial stage of the sintering process. After being sintering for a long time, the maximum pore diameter altered to a smaller value, ~1.00 μm. This value approached that measured in the pool method, which was the only one kept constant during the measurements. This might be caused by the rearrangements and slips of the α-$LiAlO_2$ particles, which occur at high temperatures and under a high stacking pressure and thermal expanding stress (thermal cycle) in the MCFC [20]. That is, the external forces (including stacking pressure and thermal stress) on a α-$LiAlO_2$ particle in a local region with a higher porosity in the matrix become unbalanced and push the particles to slip in one direction, as revealed in Fig. 6. A slip moment on an end of the α-$LiAlO_2$ particle, together with a rotation, will complete a rearrangement of the particles [21]. Thus, the

Table 2
The results of measurement and calculation of matrix porosity with sintering time

Sintering time (h)	1	500	1000	10000	20000	30000	40000
δ_E (%)	56.04	56.18	56.31	58.71	61.37	64.04	66.70
δ_W (%)	55.33	55.43	55.52	57.21	59.09	60.96	62.84

δ_E, the porosity of the matrix sintered in the electrolyte; δ_W, the porosity of the matrix sintered without impregnating the electrolyte.

Table 3
Measured maximum pore diameter in matrix by the pool at room temperature

The thickness of the matrix (mm)	Applied gas	Measurement medium	σ (N m^{-1})	P (MPa)	D_m (μm)
0.4	N_2	Alcohol	0.02239	0.089	1.01

D_m, the maximum pore diameter in the matrix.

rearrangements of the particles are usually completed through slips. They often precede the initial stage of the sintering process. The maximum pore diameter in the matrix, 2.69 μm, was measured at the beginning of its sintering process. It changed to 1.12 μm after 350 h, and to 1.01 μm after 1720 h by rearrangements of the particles. The change in coordination between the α-$LiAlO_2$ particles could result in the rearrangement and slips of the particles [7].

3.4.2. *Effect of the rearrangement on some physical properties*

The alteration of the pore-size distribution with the sintering time in the matrix sintered without impregnating with the electrolyte is shown in Fig. 7. If Fig. 7 is enlarged in scale, the positions of the arrow symbols, which indicate clearly the maximum pore radius in the matrices, changed from about 5.4 μm in Fig. 7A to about 2.7 μm in Fig. 7E with sintering time. That is, the maximum pore diameter approaches a smaller one with the sintering time.

The rearrangements and slips of the particles in the matrices could also occur under ambient pressure of N_2 [7]. After a bigger rearrangement is completed, the stress on the particles decreases, while the rearrangement energy will be translated to the surrounding area, in which an instability and a new rearrangement will exist and develop [7]. Because the length of the surrounding area affected by the translated rearrangement energy is larger than the diameter of the particle, the rearrangement energy is dispersed in a wider area, and the new rearrangement action is generally smaller, so the maximum pore diameter will change to a smaller one due to the rearrangement and slips of the α-$LiAlO_2$ particles, as mentioned above. Therefore, the rearrangements and the slips of the particles will promote the changes of the maximum pore diameters in the matrices towards a smaller one during their sintering processes.

The same action as above will occur for the change of porosities in the matrices sintered without impregnating with the electrolyte. As a result, the porosities in the matrices sintered without impregnating with the electrolyte also increase with the sintering time via the rearrangement and slips of the α-$LiAlO_2$ particles, as shown in Fig. 5. The change in coordination among the α-$LiAlO_2$ particles facilitated instability and new rearrangement [7], which did not grow into defects in the matrix, only producing uncoordinated stacking of the α-$LiAlO_2$ particles, in which the matrix porosity was increased with the sintering time.

In Fig. 7, it can be seen that the curves become steeper from Fig. 7A–E. The data on the top of the dashed rectangles indicate the pore volume percent that corresponds to the pore-size region lying at the micropore radius region first decreased and then disappeared with the sintering time, except the remaining 2% in Fig. 7E. Those with larger pore radii (pore radius ≥10,000 Å (1 μm)) altered in the same manner as described above. Moreover, those with medium pore radii increased, and the data distribution becoming narrower and more collective with the sintering time. As shown in Fig. 7, changing of the micropores to larger ones with the sintering time are also demonstrated. The rearrangements and slips of the α-$LiAlO_2$ particles finally altered their stacking state, thus causing the α-$LiAlO_2$ microparticles to lie in large pores, which were surrounded by larger α-$LiAlO_2$ particles. Microparticles contacted with larger particles. Due to the negative curvature radius at the contacted neck of the particles, chemical potential gradients existed between the necks and the particle surfaces. Then α-$LiAlO_2$ would diffuse to the necks from the particles through the contacted interfaces and the crystal lattice, but α-$LiAlO_2$ diffused at so slow rate that the surface morphology of the matrix was almost observed unchanged by SEM during its sintering process. In addition, as the α-$LiAlO_2$ microparticles disappeared gradually, the micropores became enlarged, while contrarily some larger pores changed into smaller ones, as mentioned before. Thus, the mean pore diameter increased, leading to the narrow pore-size distribution.

3.5. *Dissolution of α-$LiAlO_2$ microparticles in the matrices*

The dissolution of the α-$LiAlO_2$ particles in the electrolyte should coexist with the rearrangements and slips in MCFC during the sintering process. Ostwald ripening is available for

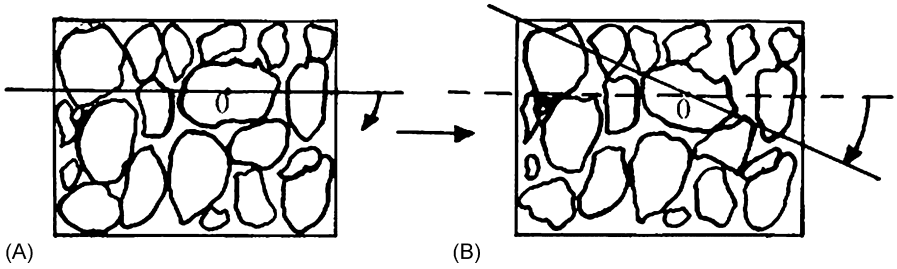

Fig. 6. A slip moment on an end of α-$LiAlO_2$ particle (0) with a rotating in an angle.

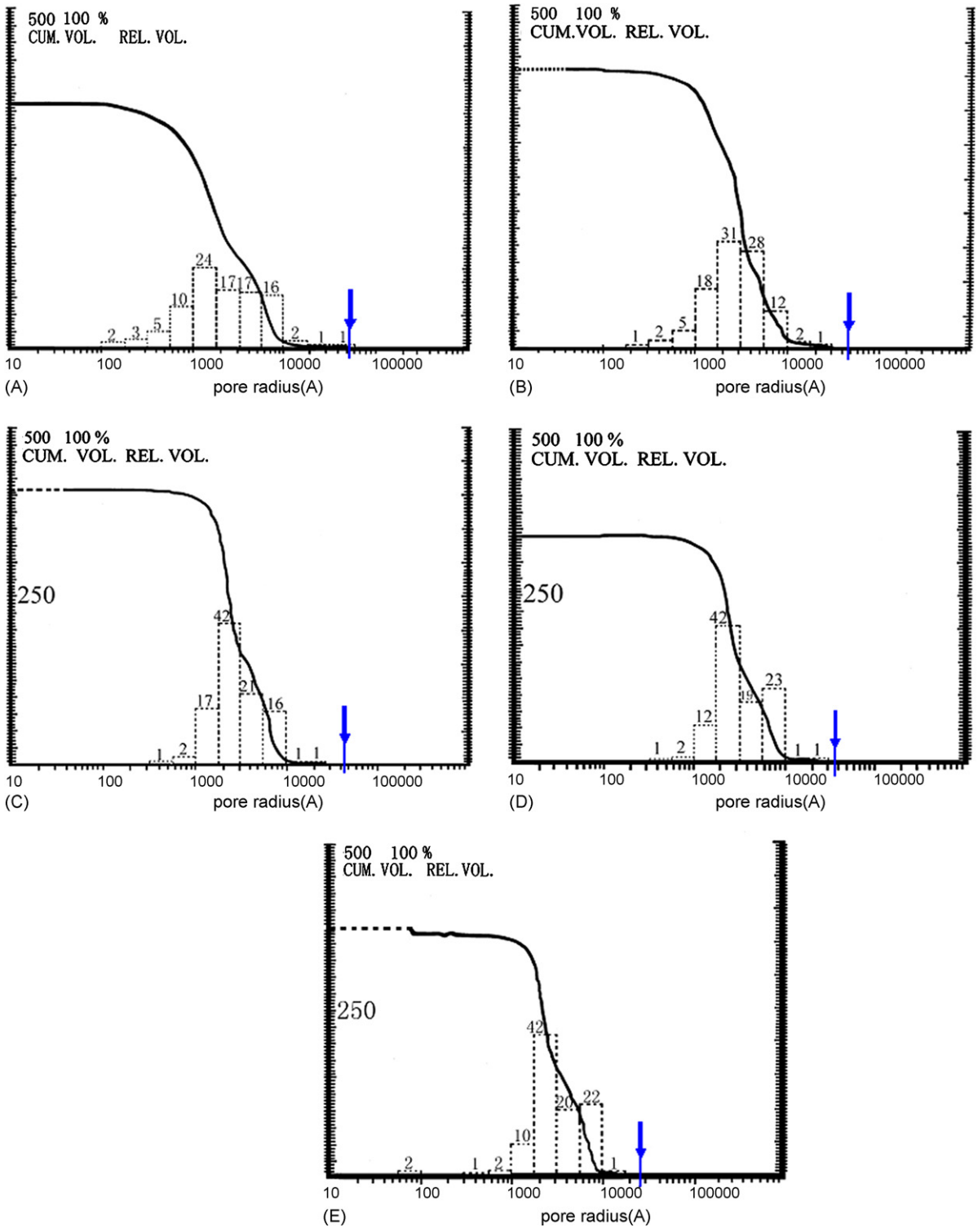

Fig. 7. (A) Pore-size distribution in the matrix sintered for 1 h without impregnating the electrolyte; (B) pore-size distribution in the matrix sintered for 1000 h without impregnating the electrolyte; (C) pore-size distribution in the matrix sintered for 2000 h without impregnating the electrolyte; (D) pore-size distribution in the matrix sintered for 3000 h without impregnating the electrolyte; (E) pore-size distribution in the matrix sintered for 4000 h without impregnating the electrolyte.

this case [22]. The Gibbs–Thomson (or Ostwald–Freundlich) equation shows the relationship between the solubility and the effective factors.

$$\ln\left[\frac{c(\gamma)}{c^*}\right] = \frac{2\phi V}{\nu k T \gamma} \tag{8}$$

where $c(\gamma)$ is the solubility of α-$LiAlO_2$ particle with radius γ. For the sake of clear presentation, the solubility of α-$LiAlO_2$ particle with radius γ was compared with that of γ-$LiAlO_2$ particle of the same radius γ as below, c^* the normal equilibrium solubility, ϕ the surface energy of α-$LiAlO_2$ particles with radius γ in contact with the electrolyte, V the molecular volume of the

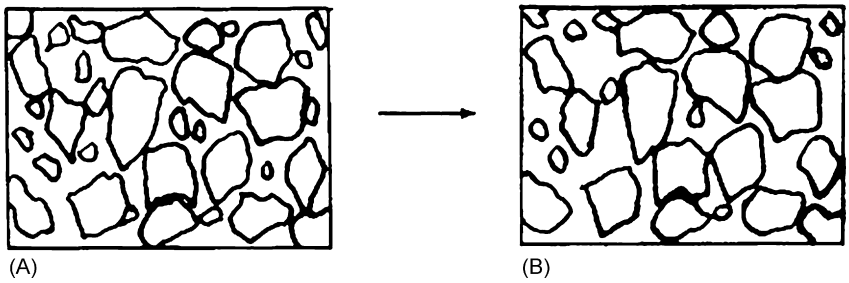

Fig. 8. Dissolution–slight deposition of some α-$LiAlO_2$ microparticles in the electrolyte.

α-$LiAlO_2$ particle, ν the number of ions in the α-$LiAlO_2$ if it is dissolved in the electrolyte, k the Boltzmann constant and T is the absolute temperature.

Since the density of the α-$LiAlO_2$ particles is higher than that of γ-$LiAlO_2$, the molecular volume of the α-$LiAlO_2$ particles is lower than that of the γ-$LiAlO_2$. So the solubility $c(\gamma)$ of the α-$LiAlO_2$ particles will be lower than that of the γ-$LiAlO_2$ with the same radius γ if the crystal defects of α-$LiAlO_2$ particles are considered to be the same as that of γ-$LiAlO_2$ [23]. More minute α-$LiAlO_2$ particles are favored to dissolve in the electrolyte at a higher dissolution rate due to its higher surface energy.

As shown in Fig. 5, the porosities in the matrices sintered in the electrolyte increased with the sintering time and were slightly higher than those in the matrices sintered without impregnating with the electrolyte. This implied that some the α-$LiAlO_2$ microparticles were dissolved in the electrolyte, while a small portion of them was migrated onto the surface of the particles. The electrolyte was kept at a lower concentration of the dissolution products of the α-$LiAlO_2$ microparticles, which were related to the size of the α-$LiAlO_2$ particles. The concentration of the dissolution products of the α-$LiAlO_2$ particles could be lower than the equilibrium deposition concentration under the experimental conditions [18]. Correspondingly, the slight deposition of the α-$LiAlO_2$ particles appeared on the neck of the contact part of two particles or on the surface of the larger particles, and this would push the dissolution–deposition reaction series forward slowly in the sintering processes.

The dissolution–slight deposition of the α-$LiAlO_2$ microparticles is depicted in Fig. 8. As shown in this figure, the matrix porosity increased with the sintering time due to the dissolution–slight deposition of the α-$LiAlO_2$ microparticles, and this is because the porosity increase of the matrices sintered in the electrolyte may result from the rearrangements of the α-$LiAlO_2$ particles and the dissolution–slight deposition of the α-$LiAlO_2$ microparticles. In contrast, those sintered without impregnating with the electrolyte were affected only by rearrangements, but not by dissolution–slight deposition. As a result of synergistic actions, the porosities in the matrices sintered in electrolyte was slightly higher than those in the matrices sintered without impregnating with the electrolyte, as shown in Fig. 5.

Accompanying the rearrangements of the α-$LiAlO_2$ particles, the dissolution–slight deposition of the α-$LiAlO_2$ microparticles resulted in an additional enlargement of the micro pore diameter and the mean pore diameter, leading to a narrow pore-size distribution in the matrices during their sintering process.

4. Conclusions

The parameters of gas obstruction ($\Delta P \geq 0.1$ MPa) and porosity ($40\% \leq \delta \leq 70\%$) are proposed as the lifetime criteria for MCFC matrices. The matrix stability can be estimated with regard to a long lifetime from two aspects—the maximum pore diameter and the porosity in the matrix, respectively, by means of regression equations derived based on the experimental results. The matrix with a good endurance should have the maximum pore diameter and porosity at the same time; otherwise the lifetime of the matrix would diminished.

The pore structure of the matrix is greatly affected by sintering. The rearrangements and slips of the α-$LiAlO_2$ particles promote the change of the maximum pore diameter towards a smaller one with sintering time in the initial stage of the sintering process. The smaller pores will change to larger ones due to the rearrangement of the α-$LiAlO_2$ particles and dissolution of some α-$LiAlO_2$ microparticles in the electrolyte, resulting in a larger mean pore diameter, and a narrow pore-size distribution in the matrices during the sintering process. The porosities in the matrices sintered in the electrolyte increased with sintering time and were slightly higher than those of matrices sintered without impregnation with electrolyte. The former was affected by the synergistic actions of the rearrangements of the α-$LiAlO_2$ particles and the dissolutions of some α-$LiAlO_2$ microparticles in the electrolyte.

Acknowledgements

The authors are thankful to Ministry of Science and Technology of China and the Chinese Academy of Sciences for the financial supports.

References

[1] L.J.M.J. Blomen, M.N. Mugerwa (Eds.), Fuel Cell Systems, Plenum Press, New York, 1993, pp. 399–414.
[2] H. Yasue, H. Kato, K. Takasu, J. Power Sources 71 (1998) 89–94.
[3] P.H. Eichenberger, J. Power Sources 71 (1998) 95–99.
[4] S.A. Hong, T.H. Lim, S.W. Nam, I.H. Oh, H.C. Lim, Korean J. Chem. Eng. 17 (2000) 193–197.
[5] N. Tomimatsu, H. Ohzu, Y. Akasaka, K. Nakagawa, J. Electrochem. Soc. 144 (1997) 4182–4186.
[6] K. Hatoh, J. Nikura, N. Taniguchi, T. Gamo, T. Iwaki, Electrochemistry (Japan) 57 (1989) 728–733.
[7] H.J. Veringa, J. Mater. Sci. 26 (1991) 5985–5995.

[8] S. Terada, I. Nagashima, K. Higaki, Y. Ito, J. Power Sources 75 (1998) 223–229.
[9] K. Nakagawa, H. Ohzu, Y. Akasaka, N. Tomimatsu, Electrochemistry (Japan) 65 (1997) 231–235.
[10] M. Murai, K. Takizawa, K. Soejima, H. Sotouchi, J. Eletrochem. Soc. 143 (1996) 2776–2783.
[11] H. Sotouchi, Y. Watanabe, T. Kobayashi, M. Murai, J. Electrochem. Soc. 139 (1992) 1127–1130.
[12] K. Takizawa, A. Hagiwara, J. Power Sources 109 (2002) 127–135.
[13] R.H. Arendt, M.J. Curran, J. Electrochem. Soc. 127 (1980) 1160–1163.
[14] H.X. Lin, L. Zhou, C.Q. He, L.Y. Kong, E.J. Zhang, B.L. Yi, Electrochim. Acta 47 (2002) 1451–1459.
[15] O. Böhme, F.U. Leidich, H.J. Salge, H. Wendt, Int. J. Hydrogen Energy 19 (1994) 349–355.
[16] H.X. Lin, B.L. Yi, N.C. Li, T.X. Qu, E.J. Zhang, L.Y. Kong, Y.C. Cheng, Electrochemistry (China) 4 (4) (1998) 406–413.
[17] C.V. Lacovangelo, W.D. Pasco, J. Electrochem. Soc. 135 (1988) 221–224.
[18] H.X. Lin, B.L. Yi, L. Zhou, C.Q. He, L.Y. Kong, E.J. Zhang, Electrochemistry (China) 6 (4) (2000) 109–119.
[19] K. Kinoshita, G.H. Kucera, J. Electrochem. Soc. 129 (1982) 216–220.
[20] M.V. Swain, Structure and Properties of Ceramics, VCH, New York/Cambridge/Tokyo/Weinheim, 1994 (Translated by J.K. Guo, et al., Science Publisher, Beijing, 1998, pp. 333).
[21] Y.-S. Kim, K.-Y. Lee, H.-S. Chun, J. Power Sources 99 (2001) 26–33.
[22] Kirk-Othmer, Encyclopedia of Chemical Technology, vol. 7, Wiley-Interscience Publication/John Wiley & Sons, New York/Chichestar/Brisbane/Toronto/Singapore, 1982, pp. 255.
[23] Y.S. Yin, J.D. Zhang, Oxide Ceramics and Multiple Material, Publisher of Chemical Industry, Beijing, 2002, pp. 72.